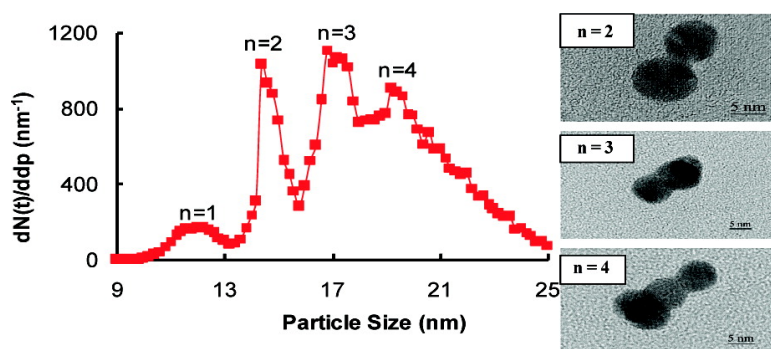# Langmuir

Article

Aggregation Kinetics of Colloidal Particles Measured by Gas-Phase Differential Mobility Analysis

D.-H. Tsai, L. F. Pease III, R. A. Zangmeister, M. J. Tarlov, and M. R. Zachariah

More About This Article

Additional resources and features associated with this article are available within the HTML version:

- Supporting Information
- Access to high resolution figures
- Links to articles and content related to this article
- Copyright permission to reproduce figures and/or text from this article

View the Full Text HTML

ACS Publications
High quality. High impact.

Aggregation Kinetics of Colloidal Particles Measured by Gas-Phase Differential Mobility Analysis

D.-H. Tsai,[†,‡] L. F. Pease III,[‡] R. A. Zangmeister,[‡] M. J. Tarlov,[‡] and M. R. Zachariah*,[†,‡]

Department of Chemistry and Biochemistry and Department of Mechanical Engineering, University of Maryland, College Park, Maryland 20742, and National Institute of Standards and Technology, Gaithersburg, Maryland 20899

Received October 11, 2007. Revised Manuscript Received April 30, 2008

We demonstrate the utility of electrospray gas-phase ion-mobility analysis as a new method to investigate nanoparticle flocculation, or aggregation. Au nanoparticle (Au-NP) solutions were sampled via electrospray (ES), followed by differential ion-mobility analysis (DMA) to determine the particle mobility distribution. Multimodal size distributions obtained with ES-DMA indicated the presence of single Au-NPs (monomer) as well as larger Au-NP clusters such as dimers, trimers, and tetramers under specific solution conditions. The fraction of each aggregate species as a function of time was quantitatively characterized, from which the degree of aggregation, aggregation rate, and stability ratio at different ionic strengths were determined. The latter enabled the extraction of a surface potential (or surface charge density) of 64 ± 2 mV for 10 nm Au-NPs, which is in good agreement with values obtained from other methods, thus validating our approach. Our results show that ES-DMA is a valuable tool for quantitatively probing the early stages of colloidal aggregation or as a preparatory tool for the size election of aggregates.

1. Introduction

Colloidal dispersions of nanoparticles have attracted attention for a variety of applications. For example, there is medical interest in using colloidal gold particles in the diagnosis and treatment of cancers.[1–3] However, the aggregation of colloidal particles represents a challenge to the development of nanotechnology and nanotherapeutics because it can affect the properties of these particles, including the transport, accessible surface area, and optical and electronic properties.[1,3,4]

DLVO theory, named after the seminal contributions of Derjaguin and Laudau and Verwey and Overbeek, provides a framework for rigorously understanding colloidal stability and aggregation.[5] This theory balances van der Waals attraction against electrostatic repulsion of like charged particles and has been used previously to characterize gold nanoparticle (Au-NP) aggregation.[6] A consideration of parameters, such as the surface potential of the particle and the Hamaker constant, is vitally important to enabling the design of engineered nanoparticles based on colloids.[5,7–15]

In this article, we present a novel method to determine the flocculation rate of colloidal particles by gas-phase analysis. Nanoparticle suspensions can be monitored by sampling the colloidal solution via electrospray (ES), thereby transforming a nanoparticle dispersion into a nanoparticle aerosol, followed by differential ion-mobility analysis (DMA) to determine the mobility distribution and thus the distribution of aggregates. By sampling the nanoparticle suspension at various times under controlled conditions, we determine the aggregation rate from which the parameters that control aggregation may be elucidated. In contrast to other techniques, such as electron microscopy[10,15] and static and dynamic light scattering (LS),[7–9,12] ES-DMA rapidly produces multimodal mobility distributions from which the proportion of each aggregation state (i.e., individual particles, dimers, trimers, tetramers, etc.) can be identified. Moreover, ES-DMA is most effective for a small number of aggregates and nanometer-sized particles (diameter <100 nm) that can often pose significant challenges to other methods.

We first present a review of the theoretical underpinnings of colloidal flocculation and describe our experimental approach. Next, we present mobility and aggregate distributions of colloidal Au-NPs determined by ES-DMA. By monitoring the distribution of aggregates as a function of ionic strength and reaction time, the flocculation mechanism (rate constant and stability ratio) and surface potential of colloidal particles are determined. Finally, dimensionless analysis is used to determine values of experimental parameters governing aggregation.

2. Theory of Brownian Aggregation of Colloidal Particles

We briefly review the DLVO model of Brownian aggregation in order to place our efforts in context and provide a foundation for our analysis.[5] Throughout the article, will use the terms flocculation and aggregation interchangeably. DVLO theory assumes that the interaction potential energy (Φ) for two spherical particles of the same size separated by a distance h (the shortest distance between two spherical particles, each having a radius of a and a center-to-center distance of r, where $h = r - 2a$) is the sum of the contributions of the electrostatic repulsive force (E_e) and the van der Waals attractive force (E_{vdw}) scaled by the Brownian thermal energy, $k_B T$, where k_B is the Boltzmann constant and T is the temperature:

* Corresponding author. E-mail: mrz@umd.edu.
† University of Maryland.
‡ National Institute of Standards and Technology.

(1) Brewer, S. H.; Glomm, W. R.; Johnson, M. C.; Knag, M. K.; Franzen, S. *Langmuir* **2005,** *21,* 9303–9307.
(2) Paciotti, G. F.; Myer, L.; Weinreich, D.; Goia, D.; Pavel, N.; McLaughlin, R. E.; Tamarkin, L. *Drug Delivery* **2004,** *11,* 169–183.
(3) West, J. L.; Halas, N. J. *Annu. Rev. Biomed. Eng.* **2003,** *5,* 285–292.
(4) Weisbecker, C. S.; Merritt, M. V.; Whitesides, G. M. *Langmuir* **1996,** *12,* 3763–3772.
(5) Russell, W. B.; Saville, D. A.; Schowalter, W. R. *Colloidal Dispersions*; Cambridge University Press: Cambridge, U.K., 1989.
(6) Kim, T.; Lee, K.; Gong, M. S.; Joo, S. W. *Langmuir* **2005,** *21,* 9524–9528.
(7) Lin, W.; Kobayashi, M.; Skarba, M.; Nu, C. D.; Galletto, P.; Borkovec, M. *Langmuir* **2006,** *22,* 1038–1047.
(8) Kobayashi, M.; Juillerat, F.; Galletto, P.; Bowen, P.; Borkovec, M. *Langmuir* **2005,** *21,* 5761–5769.
(9) Elliott, S. L.; Butera, R. J.; Hanus, L. H.; Wagner, N. J. *Faraday Discuss.* **2003,** *123,* 369–383.
(10) Dinsmore, A. D.; Weitz, D. A. *J. Phys.: Condens. Matter* **2002,** *14,* 7581–7597.
(11) Schowalter, W. R.; Eidsath, A. B. *Proc. Natl. Acad. Sci. U.S.A.* **2001,** *98,* 3644–3651.
(12) Weitz, D. A.; Lin, M. Y.; Lindsay, H. M. *Chemom. Intell. Lab. Syst.* **1991,** *10,* 133–140.
(13) Prieve, D. C.; Ruckenstein, E. *J. Colloid Interface Sci.* **1980,** *73,* 539–555.
(14) Spielman, L. A. *J. Colloid Interface Sci.* **1970,** *33,* 562.
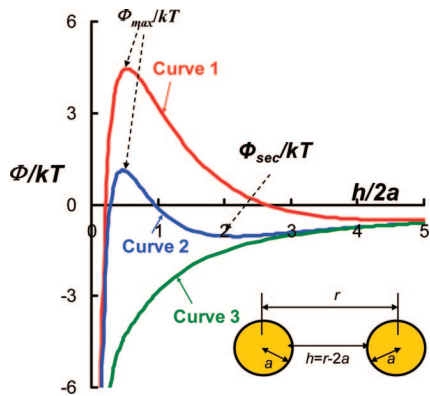(15) Enustun, B. V.; Turkevich, J. *J. Am. Chem. Soc.* **1963,** *85,* 3317.

Figure 1. Interaction potential for two spherical colloidal particles with diameters of 10 nm and a surface potential of 64 mV. Curve 1 represents particles in the reaction-limited regime ($C = 1$ mmol/L), curve 2 represents particles in the intermediate regime ($C = 3$ mmol/L), and curve 3 represents particles in the diffusion-limited regime ($C = 20$ mmol/L). The radius of the particles is a, the center-to-center distance between two particles is r, $h = r - 2a$, and the salt concentration is C.

$$\frac{\Phi}{k_B T} = \frac{1}{k_B T}(E_e + E_{vdw}) \tag{1}$$

The electrostatic repulsive force of the electric double layers on adjacent particles is dependent on the surface potential, Ψ_s, modulated by the ionic strength of the solution following Debye−Hückel theory (where the Debye−Hückel length, λ_D, is approximated as ~0.305 nm/$\sqrt{n_s}$, and n_s is the ionic strength in mol/L [16]). This relationship can be summarized by eq 2

$$E_e = B_1 \exp(-\kappa h) \tag{2}$$

where $B_1 = 8ak_B T/z^2 l_b \tanh^2(ez\psi_s/4k_B T)$ for two spheres under superposition and constant potential conditions without linearization,[5] $\kappa = 1/\lambda_D$, and z is the charge of the solvated ion. The Bjerrum length, $l_b = e^2/4\pi\varepsilon_0\varepsilon_r k_B T$, depends on the permittivity of free space, ε_0, the magnitude of the electron charge, e, and the relative permittivity of water, ε_r.

The van der Waals force of attraction between adjacent particles is summarized in equation 3:

$$E_{vdw} = -\frac{B_2}{h} \tag{3}$$

where $B_2 = aA_{eff}/12$ under the Derjaguin approximation in the nonretarded limit,[5] where the Hamaker constant, A_{eff}, is 3.0×10^{-19} J for Au-NP in water.[5]

Figure 1 is a plot of the potential energy, $\Phi/k_B T$, versus the scaled separation distance, $h/2a$, between two spherical Au-NPs under three conditions: the reaction-limited (curve 1), intermediate (curve 2), and diffusion-limited (curve 3) regimes. Irreversible flocculation occurs as two particles approach each other and fall into the primary minimum near $h = 0$. In the reaction-limited regime, the sum of E_e and E_{vdw} creates both a maximum, $\Phi_{max}/k_B T$ near $r = 2a + \lambda_D$,[5] and a secondary minimum, $\Phi_{sec}/k_B T$, at relatively large particle separation, $h = r_{sec}$. The height difference between these two provides an energy barrier to minimize or prevent flocculation. We note that additional non-DLVO forces arise when the maximum is located less than 1 nm from the particle surface. This situation is not encountered in the present experiments because of the large Hamaker constant of gold.[5,17]

(16) Andelman, P. *Soft Condensed Matter Physics in Molecular and Cell Biology*; Taylor & Francis: New York, 2006.

(17) Behrens, S. H.; Christl, D. I.; Emmerzael, R.; Schurtenberger, P.; Borkovec, M. *Langmuir* 2000, *16*, 2566–2575.

A dimensionless energy barrier to Brownian flocculation, E_a^*, can be defined as

$$E_a^* = \frac{1}{k_B T}(\Phi_{max} - \Phi_{sec}) \tag{4}$$

where Φ_{max} and Φ_{sec} are the maximum and minimum in the energy as a function of interparticle separation (Figure 1). Φ_{max} may be approximated by setting the interparticle separation equal to λ_D, giving

$$\frac{\Phi_{max}}{k_B T} = \frac{1}{k_B T}\left(0.37B_1 - \frac{B_2}{\lambda_D}\right) \tag{5}$$

and we will determine Φ_{sec} momentarily. For highly stable suspensions (i.e., the reaction-limited regime), $|\Phi_{max}| \gg |\Phi_{sec}|$ such that $E_a^* \approx \Phi_{max}/k_B T$. Conversely, in the diffusion-limited regime (curve 3), neither $\Phi_{max}/k_B T$ nor $\Phi_{sec}/k_B T$ is significant, such that the energy barrier is negligible or nonexistent. In the intermediate regime (curve 2), both $\Phi_{max}/k_B T$ and $\Phi_{sec}/k_B T$ possess similar magnitudes, so $\Phi_{sec}/k_B T$ cannot be ignored in the evaluation of E_a^* in contrast to the reaction-limited regime.

Because the intermediate regime is essential to our subsequent analysis, we now provide an approximate expression for Φ_{sec} that depends on the separation of the particles, r_{sec}, through eq 6. Intuitively, we should be able to take the first derivative of eq 1 (i.e., set $d(\Phi/k_B T)/dh = 0$); however, this results in a transcendental expression for r_{sec}. To circumvent this difficulty, we numerically calculated $\exp(-h/\lambda_D)$ for the intermediate regime where $2\lambda_D < h < 5\lambda_D$. In this domain, we find $1.26(h/\lambda_D)^{-3}$ to be a sufficiently precise power law approximation for $\exp(-h/\lambda_D)$, enabling an analytical solution for r_{sec}. Thus, eq 1 becomes

$$\frac{\Phi}{k_B T} = \frac{1}{k_B T}\left(1.26B_1\kappa^{-3}h^{-3} - \frac{B_2}{h}\right) \tag{6}$$

Now setting the first derivative of eq 6 equal to zero gives $r_{sec} = \sqrt{3.78B_1\lambda_D^3/B_2}$. The energy barrier, E_a^*, of eq 4 then becomes

$$E_a^* = \frac{1}{kT}\left(1.26B_1 - \frac{B_2}{\lambda_D} + 0.343\sqrt{\frac{B_2^3}{B_1\lambda_D^3}}\right) \tag{7}$$

in the intermediate regime. Generally, E_a^* is affected by several variables including ionic strength, particle size, and surface potential, each of which can be measured or fixed in the present study. The remainder of this article demonstrates how to obtain relationships among these variables in the intermediate regime with DLVO theory using ES-DMA measurements of the temporal distribution of cluster sizes.

3. Experiment

Electrospray (ES) of colloidal particles from solution is an effective way to aerosolize individual colloidal particles for DMA. Although the ES of colloidal particles[18−20] has been demonstrated recently, the studies reported here, to our knowledge, represent the first demonstration of ES-DMA characterization of the aggregation kinetics of colloidal particles in solution.

3.1. Materials. Commercially available monodisperse Au colloids (nominally 10 nm in diameter, citrate-stabilized, Ted Pella Inc.) were used in this work. The Au colloid suspension was first centrifuged to separate the colloids from the supernatant containing excess citrate ions. The supernatant was removed (typically 0.95 mL of a 1.00 mL

(18) Bottger, P. H. M.; Bi, Z.; Adolph, D.; Dick, K. A.; Karlsson, L. S.; Karlsson, M. N. A.; Wacaser, B. A.; Deppert, K. *Nanotechnology* 2007, *18*.

(19) Lenggoro, I. W.; Lee, H. M.; Okuyama, K. *J. Colloid Interface Sci.* 2006, *303*, 124–130.

(20) Lenggoro, I. W.; Xia, B.; Okuyama, K.; de la Mora, J. F. *Langmuir* 2002, *18*, 4584–4591.

sample) and replaced with an equivalent volume of ca. 2−10 mmol/L aqueous ammonium acetate (Sigma, 99.9%) solution. Replacing the citrate salts with the more volatile ammonium acetate allows for systematic variation of the ionic strength while minimizing the thickness of any nonvolatile salt residues that may dry on the surface of the colloid and broaden the detected size distribution. The concentration of ammonium acetate was varied from 2.12 to 9.47 mmol/L to avoid rapid flocculation (seconds) so that experiments could be performed on a reasonable time scale (days). Though this concentration range is rather modest, it spans the intermediate regime and was found to dramatically affect the kinetics of flocculation on the time scale of our experiments (∼ 20 min).

3.2. Electrospray Particle Generation and Differential Mobility Analysis. Figure 2 depicts a schematic of our experimental system, consisting of an electrospray aerosol generator (model 3480, TSI Inc.), a differential mobility electrode column (model 3080n, TSI Inc.), and a condensation particle counter (CPC, model 3025, TSI Inc.). Flow handling, interfacing among the instruments, and mobility data reduction were done in house. Within the electrospray aerosol generator, conductive solutions of Au colloids were placed in the pressure chamber and then delivered to a nozzle through a capillary (0.025 mm in diameter, 24 cm in length, TSI Inc.). The liquid flow rate in the capillary, Q_1, was ∼66 nL/min, and the flow rate of carrier gas outside of the nozzle was 1.2 L/min. To achieve better electrical stability in the ES, filtered air was augmented with CO_2 (83 volume % air and 17% CO_2) to increase the dielectric breakdown threshold. Operating with an applied voltage of 2 to 3 kV, we sprayed the Au colloids in cone-jet mode, which is characterized by a meniscus in the form of a sharp and ostensibly time-invariant Taylor cone. The aerosol stream is then passed through a housing containing a radioactive Po-210 (α) source that reduces the highly charged droplets emerging from the Taylor cone to droplets that are primarily either neutral, have a single negative charge, or have a single positive charge. The positively charged dry particles were separated within the differential mobility analyzer on the basis of their electrical mobility, which is inversely proportional to the projected area of the Au particles, d_p^2.[21−25] The differential mobility analyzer acted as a narrow band-pass filter, transmitting aerosolized colloids of a specific mobility or size to a condensation particle counter (CPC). Within the CPC, the particles nucleate a much larger droplet in a saturated butanol environment that can easily be detected with light scattering, and the number of droplets (independent of their size) passing a detector is reported. To achieve sufficient resolution and stability from the DMA, the ratio of sheath-to-aerosol flow rates within the DMA was set to 30. Under these conditions, data were collected with a scanning step size of 0.2 nm for 20 s because the uncertainty contributed by the DMA remains less than 0.3 nm.[21,22,26] Thus, the width of the peaks in the resulting mobility spectra results primarily from the distribution in particle size.

The mobility diameter distribution of the Au-NP clusters was obtained from the ion-mobility spectrum for positively charged particles by correcting each data point for the charging efficiency. The charge distribution is particle-size-dependent and can be described using a modified Boltzmann distribution.[27] The charging efficiency is the ratio of singly charged, positive particles to the total number of particles in the gas phase.[28,29] For example, the CPC count at 10 nm size is multiplied by ∼24 to account for the fact that 4.1% of the particles are positively charged, whereas that at 15 nm
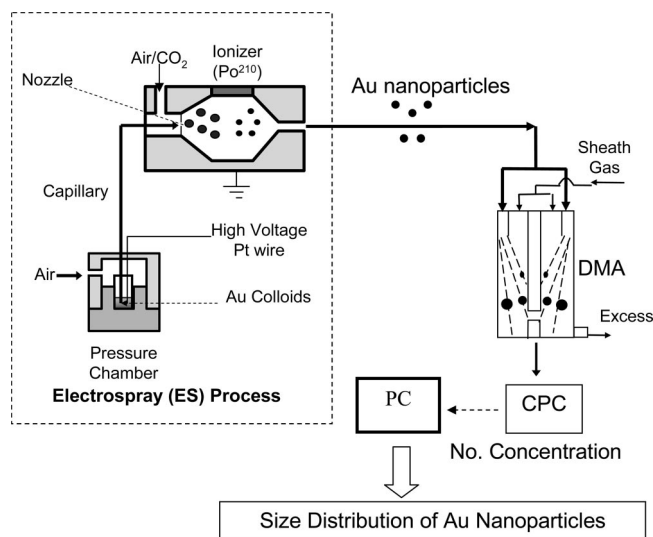

Figure 2. Schematic of the ES-DMA used to measure particle size distributions, including the electrospray (ES), differential mobility analyzer (DMA), and condensation particle counter (CPC).

size is multiplied by ∼16 to account for the fact that only 6.4% of 100 particles are positively charged. Hereafter, we define *n* as the number of primary particles (termed monomers, $n = 1$) contained in an aggregate ($n = 2$ for a dimer, $n = 3$ for a trimer, and $n = 4$ for a tetramer), and $d_{p,n}$ as the mobility diameter of *n*mer clusters. It took approximately 17 min from the moment the particles were mixed until the instrumentation began to record the spectrum. This delay was due to the time needed to insert the sample into the instrument, transit the dead volume within the capillary, establish the electrospray, and begin detecting particles.

The identity of particles or particle clusters in each multimodal peak was confirmed with transmission electron microscopy (TEM). Particles or clusters of a particular size or mobility were selected by diverting the output of the DMA to an electrostatic deposition chamber (TSI 3089). There the selected particles were deposited onto a carbon film. These particles were then analyzed with TEM.

By integrating the peaks for each *n*mer in the mobility diameter distribution,[29,30] the number of Au particles in different aggregation states $N_{c,n}$, was determined from ES-DMA by

$$N_{c,n} = \left[\int_{d_{p,n,\min}}^{d_{p,n,\max}} \frac{dN_{g,n}}{dd_p} \, dd_p \right] \times \frac{Q_g}{Q_1} \quad (8)$$

where $N_{g,n}$ is the measured concentration of Au-NP in the gas phase, Q_1 is the liquid flow rate through a capillary (= 66 nL/min), Q_g is the gas flow rate (= 1.2 L/min), and $d_{p,n,\max}$ and $d_{p,n,\min}$ are the maxima and minima mobility diameters bounding a peak corresponding to an *n*-mer cluster, respectively.

4. Results and Discussion

Our objective is to develop a systematic approach to detect the liquid-phase aggregation of nanoparticles using ES-DMA. We restrict the scope of this article to the early stage of aggregation where individual nanoparticles form small clusters (<5 primary particles) prior to significant cluster−cluster aggregation, though given sufficient number concentration this approach can be extended to arbitrarily sized aggregates (as in diffusion-limited aggregation[9,12]). The suspensions we employ herein are dilute suspensions, containing fewer than 10^{13} particles/mL (0.1 mg/mL) for a volume fraction of ∼10^{-6}.

Although it is possible for aggregation to occur in the gas phase, the particle concentration both within the aerosolized

(21) Tsai, D-H, Z. R. A.; Pease, L. F.; Tarlov, M. J.; Zachariah, M. R. *Langmuir* **2008**, *24*(16), 8483–8490.

(22) Pease, L. F.; Tsai, D. H.; Zangmeister, R. A.; Zachariah, M. R.; Tarlov, M. J. *J. Phys. Chem. C* **2007**, *111*, 17155–17157.

(23) Pease, L.F., III; Tsai, T.-D.; Zangmeister, R. A.; Hertz, J. L.; Zachariah, M. R.; Tarlov, M. J. *Manuscript*, 2007.

(24) Kim, S. H.; Mulholland, G. W.; Zachariah, M. R. *J. Aerosol Sci.* **2007**, *38*, 823–842.

(25) Kim, S. H.; Zachariah, M. R. *Nanotechnology* **2005**, *16*, 2149–2152.

(26) Liao, Y. C.; Roberts, J. T. *J. Am. Chem. Soc.* **2006**, *128*, 9061–9065.

(27) Wiedensohler, A. *J. Aerosol Sci.* **1988**, *19*, 387–389.

(28) Kim, S. H.; Woo, K. S.; Liu, B. Y. H.; Zachariah, M. R. *J. Colloid Interface Sci.* **2005**, *282*, 46–57.

(29) Hind, W. C. *Aerosol Technology*, 2nd ed.; Wiley-Interscience: New York, 1998.

(30) Hogan, C. J.; Kettleson, E. M.; Ramaswami, B.; Chen, D. R.; Biswas, P. *Anal. Chem.* **2006**, *78*, 844–852.
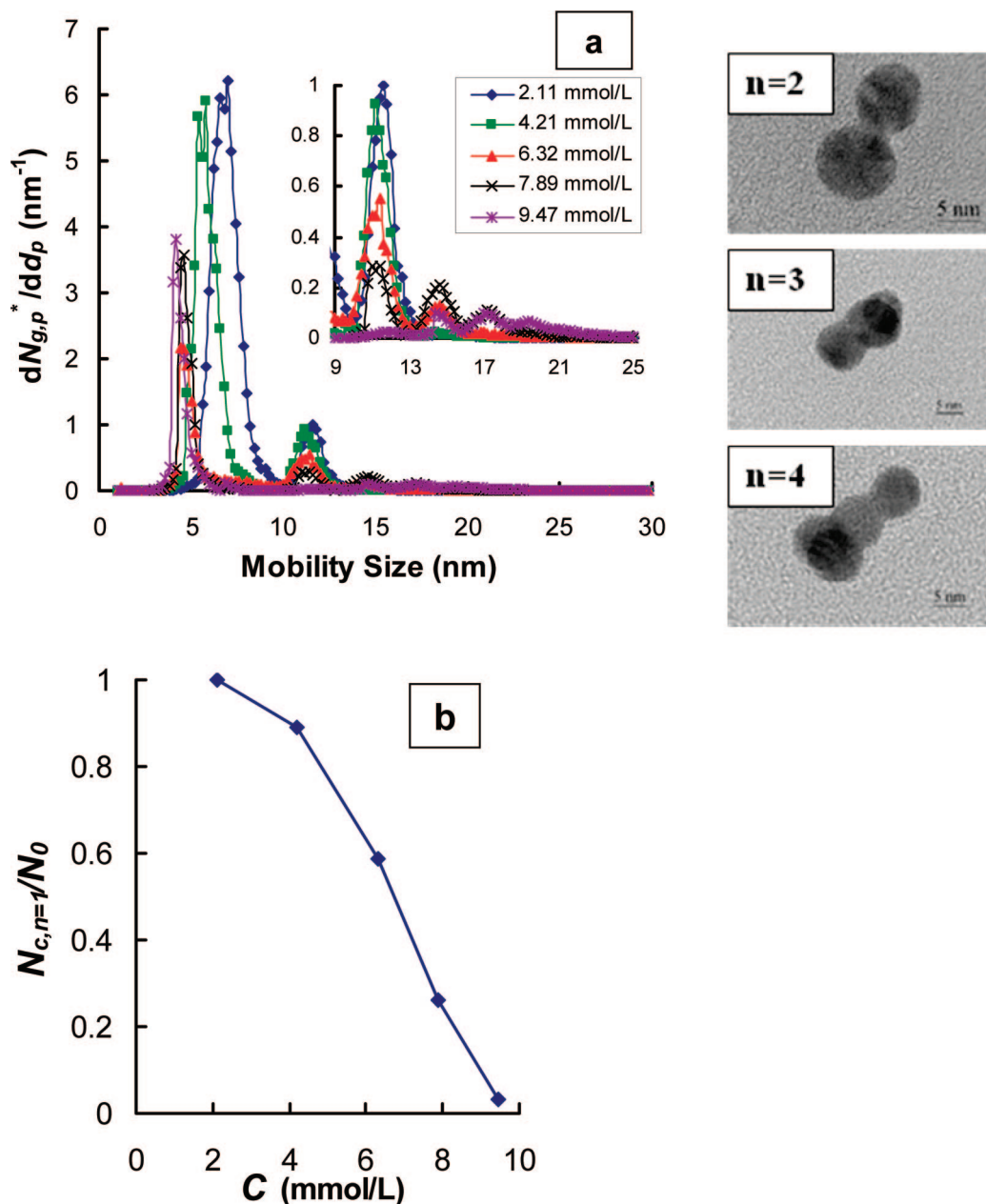
Figure 3. (a) Ion-mobility spectra of Au-NPs nominally 10 nm in diameter in ammonium acetate solutions of varying concentration. (b) Fraction of primary particles remaining, $N_{c,n=1}/N_0$, corresponding to panel a versus ionic strength. $N_{g,n}$ is the number concentration of Au particles measured by DMA-CPC in the gas phase ($N_{g,n}{}^* = N_{g,n}/N_0$), N_0 is the initial concentration of monomer Au particles, and n is the number of single particles in a Au aggregate. The volumetric fraction of Au-NP in solution is $\sim 10^{-6}$, and the distributions were sampled at a reaction time of $t \approx 20$ min.

droplet (0.04 particles per droplet) and in the gas phase (at most 10^6 particles/cm^3) is sufficiently dilute and the residence time (<10 s in the gas phase) is sufficiently short to prevent significant aggregation. Similarly, it is possible for shear forces within the electrospray capillary to induce flocculation, but this effect is calculated to be negligible as a result of the low flow velocity (~ 2 mm/s) used. Thus, we believe that the observed aggregates reflect aggregation in the liquid phase prior to analysis. Indeed, unless we intentionally force aggregation by adding salts, the fraction of aggregated particles is typically near or below the detection limit by ES-DMA. Only upon addition of salts does the solution change color from a bright red to a purple or blue color, characteristic of aggregated gold clusters.[4]

We first identify the peaks in the ion-mobility spectrum and then proceed to examine the time-dependent kinetic behavior of aggregation. From a temporal change in the number concentration of each aggregation state, we estimate the rate of aggregation of

Au-NPs. From this, we estimate the surface potential of the Au-NPs and compare it to surface potentials measured by other methods to confirm the validity of our results.

4.1. Effect of Ionic Strength. Figure 3 presents ion-mobility spectra of nominally 10-nm-diameter Au-NPs at various concentrations of ammonium acetate, C. We note that for a 1:1 electrolyte such as ammonium acetate the ionic strength is equivalent to concentration. Each spectrum exhibits up to five distinctive peaks representing clusters containing one to five individual Au particles, which we term monomer, dimer, trimer, and so forth. The ion-mobility peak at 11.6 nm is assigned to the monomer ($n = 1$), which is consistent with the nominal size of the as-received Au-NP sample encrusted with salts.[21] The peaks centered at 14.8, 17.4, and 19.4 nm are assigned to dimers, trimers, and tetramers, respectively. These assignments were confirmed by depositing particles corresponding to each peak exiting the DMA on a TEM grid inside an electrostatic deposition

chamber (e.g., the peak labeled as a tetramer was found to consist of four Au-NPs).[23]

Figure 3a shows how the concentration of each cluster or aggregate varies with salt concentration. As seen in Figure 3a, the intensity of the monomer ($n = 1$) decreases, and the intensities of the dimer ($n = 2$), trimer ($n = 3$), and tetramer ($n = 4$) increase as C increases, reflecting the decreased electrostatic repulsion between Au-NPs due to a decrease in the Debye screening length with added salts. Importantly, these results indicate that ES-DMA can clearly resolve the aggregate distribution in solution and monitor changes in the distribution due to solution conditions.

Figure 3b further quantifies the effect of ionic strength on the extent of aggregation. Here we define the normalized monomer concentration, $N_{c,n=1}/N_0$, where N_0 is the initial monomer concentration (4.6×10^{11} particles/cm³). Low ammonium acetate concentrations (i.e., $C = 2.12$ mmol/L) result in stable colloids where $N_{c,n=1}/N_0 = \sim 1$ (i.e., the dominant species are Au-NP monomers ($n = 1$)). As the salt concentration increases, significant quantities of dimers and trimers are observed. Upon increasing the salt concentration to $C = 9.47$ mmol/L, $N_{c,n=1}/N_0 < 0.1$ and few monomers are observed. Our measurements are in excellent qualitative agreement with the predictions of DLVO theory.[5,7−15] Thus, ES-DMA is particularly sensitive for the detection of nanoparticle aggregates (<100 nm) in the early stages of flocculation. Next we show that changes in these distributions can be monitored as a function of time to study the aggregation kinetics.

4.2. Time-Dependent Kinetic Study and Degree of Flocculation. The results in Figure 3 depend on when the flocculating solution is sampled, a fact we now exploit to determine the kinetics of flocculation. To quantify the extent of flocculation, we draw an analogy between the flocculation of colloidal particles and a step-growth polymerization process to define the degree of flocculation (DF)

$$\text{DF} = \frac{\sum_n n N_{c,n}}{\sum_n N_{c,n}} \quad (9)$$

In this analogy, each NP corresponds to a repeat unit, and a cluster of n NPs corresponds to a polymer chain of length n. The flocculation is treated much like a polymer propagation process where the average number of particles per aggregate or the degree of aggregation, DF, increases from unity as a function of reaction time, t.[31]

Figure 4 characterizes the extent of Au-NP flocculation versus time. At an ammonium acetate concentration of 2 mmol/L (Figure 4a-1), only monomer particles were observed after 9 days, indicating that repulsive forces dominate on the experimentally accessible time scale. Hence, the energy barrier, characterized in Figure 1, is high, and flocculation is reaction-limited when C < 2.12 mmol/L. At $C = 4.21$ mmol/L (Figure 4a-2), monomer particles still comprise the major species, but the concentration of monomer is observed to decrease with time whereas the concentrations of dimers and trimers increase. When C is increased to 7.89 mmol/L (Figure 4a-3), flocculation is very much enhanced as evidenced by both the high concentration of the various $n$mers relative to the monomer and the much shorter experimental times for monomer Au-NP. (The half-life, $t_{1/2}$, decreased from days to minutes. See Table 1.)

Figure 4b displays the relative fraction of each Au-NP species as a function of reaction time at an ammonium acetate concentration of 7.89 mmol/L. Consistent with simple Brownian

flocculation, the monomer concentration decreases exponentially with each successive $n$mer appearing later in time. For this set of experimental conditions, dimers and trimers reached a peak concentration at $t \approx 80$ and 200 min, respectively. Note that the defined reaction time starts from the moment Au colloids were mixed with ammonia acetate buffer solution until the time the ion-mobility spectrum was collected. The trend observed in Figure 4b is consistent with Smoluchowski's theory, showing a monotonic decrease in monomer and a maximum concentration of n-mers versus time where $n > 2$.[5,32]

Figure 4c shows the average number of particles per cluster or the degree of flocculation, DF, versus reaction time, t, for various ammonium acetate concentrations. Generally, a higher DF was observed for longer reaction times and higher ammonium acetate concentrations. Because of the depletion of Au-NP monomer at $C = 9.47$ mmol/L, DF approaches a constant at $t > 80$ min. This result indicates that the flocculation rate is dominated by monomer/n-mer interactions such that when the monomer is depleted aggregation essentially stops. This implies that aggregate−aggregate coagulation is too slow to play a significant role for the time scales and concentration ranges considered here.

4.3. Determination of the Rate-Determining Step. Using the curves in Figure 4b, we now examine the kinetics of aggregation. We draw upon the irreversible population balance equation[32] attributed to Smoluchowski and assume the rate constants, k_D (or coagulation coefficients), to be particle-size-independent. Using this assumption, we write

$$\frac{dN_{\text{total}}(t)}{dt} = -k_D[N_{\text{total}}(t)]^2 \quad (10)$$

where k_D is the lumped rate constant and $N_{\text{total}}(t) = \sum_{n \equiv 1}^{n \equiv \infty} N_{c,n}(t)$ is the total number of Au-NP clusters ($\leq N_0$, the total number of primary particles at $t = 0$). Integration leads to

$$N_{\text{total}}(t) = \frac{N_0}{1 + k_D N_0 t} \quad (11)$$

This expression is used to plot the decay of $N_{\text{total}}(t)$ with t as shown in Figure 5. Increasing the ionic strength causes $N_{\text{total}}(t)$ to decay more sharply. This result is consistent with an Arrhenius form of the rate constant,

$$k_D = A_o e^{-E_a^*/k_B T} \quad (12)$$

which depends on both a collision frequency, A_o, and an activation barrier, E_a. As mentioned in section 2, the activation barrier for flocculation depends on the energy barrier between the secondary minimum ($\Phi_{\text{sec}}/k_B T$) and maximum ($\Phi_{\text{max}}/k_B T$). As the salt concentration rises, the electrostatic barrier collapses, and the rate constant should likewise increase. Fitting the curves in Figure 5 leads to rate constants of $k_D \approx 10^{-17}$ cm³/s for $C = 4.21$ mmol/L, $k_D \approx 8 \times 10^{-17}$ cm³/s for $C = 6.32$ mmol/L, $k_D \approx 2 \times 10^{-15}$ cm³/s for $C = 7.89$ mmol/L, and $k_D \approx 4 \times 10^{-15}$ cm³/s for $C = 9.47$ mmol/L. Comparing these rate constants with a diffusion-limited rate constant (k_D^{fast}) value of $\sim 10^{-11}$ cm³/s for 10-nm-sized Au-NP's[7,32] indicates that electrostatic repulsion decreases the flocculation rate by $10^3−10^6$.

From the rate constants, we can determine the energy barrier to flocculation in the primary minimum. First, we cast our experimental results into a dimensionless stability ratio,

$$W \equiv \frac{k_D^{\text{fast}}}{k_D} \quad (13)$$

as defined by Lin et al.,[5,7] which compares the flocculation rate

(31) Sandler, S. R. *Polymer Synthesis II*; 1977.

(32) Friedlander, S. K. *Smoke, Dust, and Haze: Fundamentals of Aerosl Dynamics*, 2nd ed.; Oxford University Press: New York, 2000.
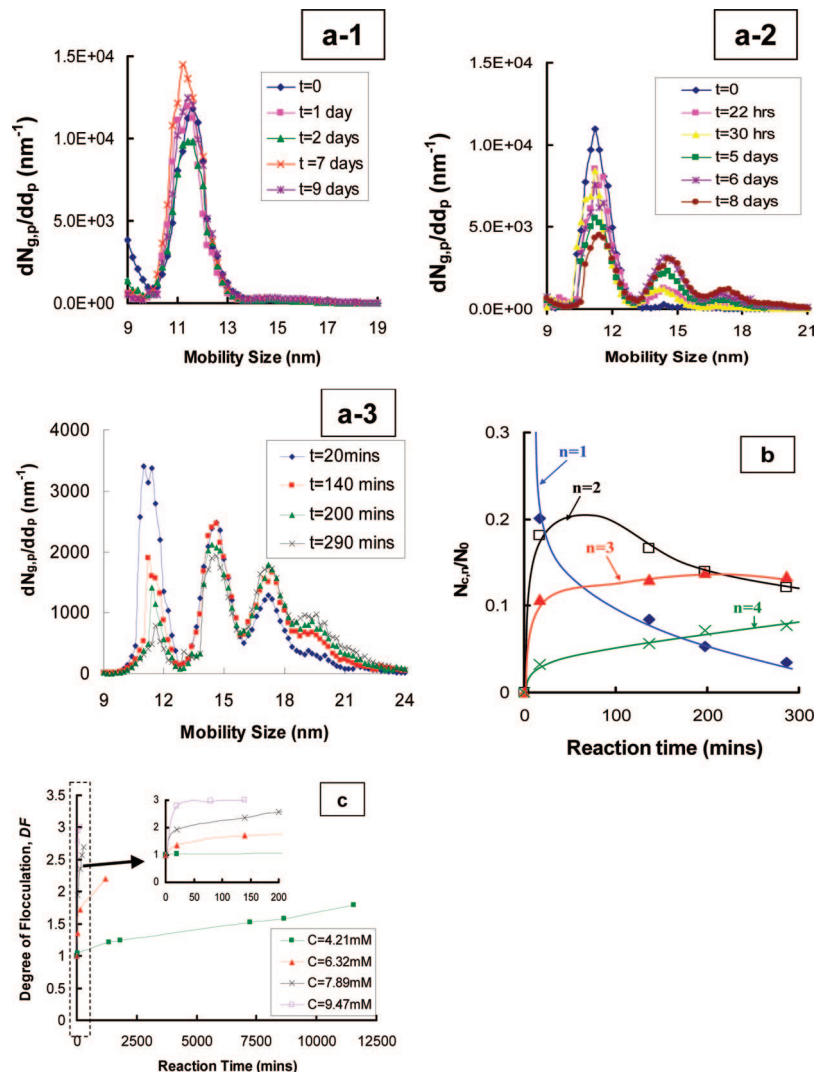
Figure 4. Ion-mobility spectra of nominally 10-nm-diameter Au-NPs at various reaction times, t, after adjusting the solution concentration (C) of ammonium acetate to (a-1) 2.12, (a-2) 4.21, and (a-3) 7.89 mmol/L. (b) Normalized concentration of aggregates containing 1 ($\blacklozenge$), 2 ($\square$), 3 ($\blacktriangle$), or 4 ($\times$) primary particles vs reaction time at C = 7.89 mmol/L, where $N_{c,n}$ is the number concentration of Au-NP in solution, and n is the number of individual particles per aggregate. (c) Average number of particles per aggregate or degree of flocculation, DF, vs reaction time for ammonium acetate concentrations, C, of 4.21 to 9.47 mmol/L.
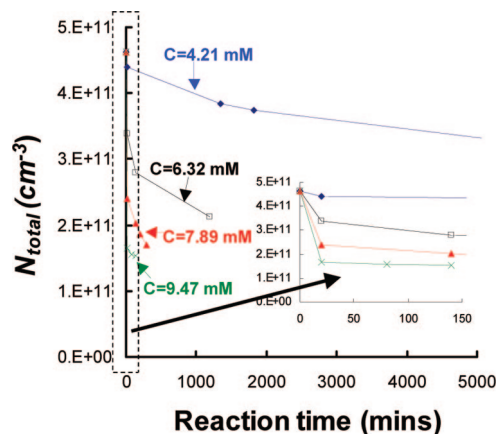

Figure 5. Total number concentration of Au-NPs aggregates in solution, N_{total}, vs reaction time, t, for four ammonium acetate concentrations.
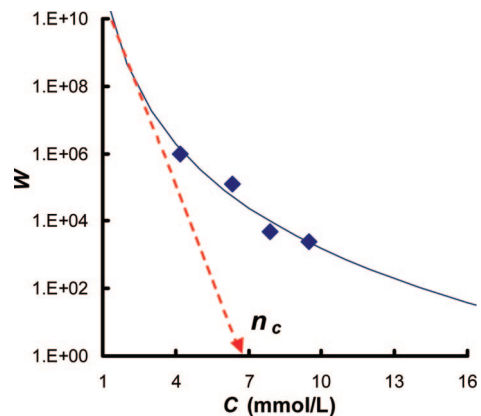

Figure 6. Stability ratio of Au colloids plotted against ionic strength. Note that for the 1:1 electrolye ammonium acetate used in this study concentration and ionic strength are equivalent. Extrapolation to the x axis (red arrow) determines the critical concentration of salt, n_c, needed for the flocculation of Au colloids.

driven solely by Brownian motion to the experimentally observed flocculation rate. Larger values of W correspond to more stable suspensions. Plotting W versus the ionic strength in Figure 6 clearly shows a monotonic decrease in W with C. The data in the Figure has been fit with the functional form of a power law

as indicated by Prieve and Ruckenstein.[13] By extrapolation of the data to the x axis, we obtain the critical salt concentration, n_c, to induce Au-NP flocculation (6.5 $\pm$ 1.0 mmol/L). Notably,
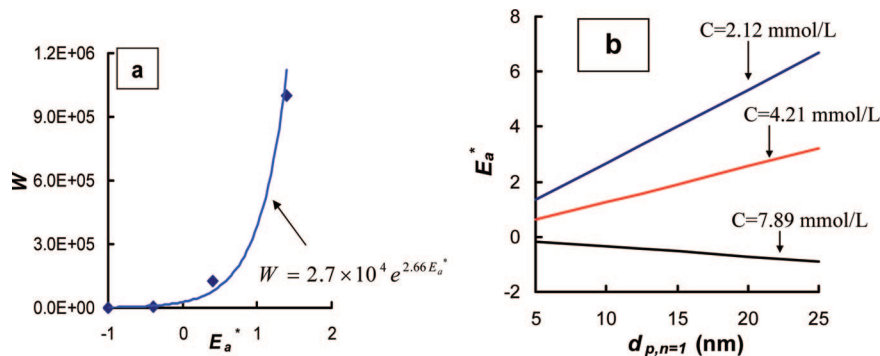
Figure 7. (a) Dimensionless analysis comparing the stability ratio, W, with the height of the energy barrier, E_a^*. (b) The height of the energy barrier, E_a^*, obtained using eq 6 assuming a constant surface charge density of 0.075 e/nm^2 versus the primary particle size, $d_{p,n=1}$.

Table 1. Half-Life of Primary Particles ($n = 1$) versus Salt Concentration

salt concentration (mmol/L)	$t_{1/2}$
2.12	>9 days
4.21	~5 days
6.32	~17 min
7.89	<17 min
9.47	<17 min

Note that the detection limit of $t_{1/2}$ is approximately 17 min as a result of the time needed to insert the sample into the instrument, transit the dead volume within the capillary, establish the electrospray, and begin detecting particles.

n_c provides an estimate of the onset of rapid flocculation.[5]

This value of n_c enables the determination of the surface potential between two Au-NPs, Ψ_s, and the surface charge density of individual Au nanoparticles, Q_s, through the following equations:[5]

$$|\psi_s| = \frac{4kT}{ez}\left(\text{arctanh}\left[\frac{n_c z^6 l_b{}^3 A_{\text{eff}}{}^2}{49.6(k_B T)^2}\right]^{1/4}\right) \quad (14)$$

$$|Q_s| = \varepsilon_0 \varepsilon_r \kappa |\psi_s| \quad (15)$$

Applying these relationships finds $|\psi_s|$ to be 64 ± 2 mV. This magnitude may be compared with the linear trend in zeta potential versus the diameter of citrate-stabilized gold measured using a commercial electrophoresis instrument by Kim et al.[6] Extrapolating their data to 10 nm finds Ψ_s to be -65 mV. The excellent agreement validates ES-DMA as a tool for studying colloidal stability quantitatively.

With further application of eq 15, we find Q_s to be ~0.012 C/m^2 (= 0.075 e/nm^2), indicating the average number of elementary charges on the monomer ($d_{p,n=1} = 10.9$ nm) to be ~28. Substituting Ψ_s back into eqs 4−6 yields $E_a \approx 1.4kT$ for $C = 4.21$ mmol/L, $E_a \approx 0.4kT$ for $C = 6.32$ mmol/L, $E_a \approx -0.4kT$ for $C = 7.89$ mmol/L, and $E_a \approx -1.0kT$ for $C = 9.47$ mmol/L. Because diffusion-limited flocculation is defined as $E_a \ll kT$, the boundary between diffusion-limited and reaction-limited regimes lies in the salt concentration range of ~6−8 mmol/L. Thus, we conclude that the Au-NPs experience intermediate values of the interactive potential as illustrated in Figure 1 for the range of salt concentrations employed in these experiments ($C = 4.21-9.47$ mmol/L).

4.4. Dimensionless Analysis. We now summarize our analysis and characterization by demonstrating how to extend our analysis to other cases with DLVO theory. Having determined the surface charges via the critical salt concentration, we now return to eq 6 to determine the height of the energy barrier. Following the analysis by Prieve and Ruckenstein,[5,13] Figure 7 shows that the stability ratio increases exponentially with the height of the energy barrier, consistent with the theory that increasing the energy barrier of

flocculation improves the stability of primary colloidal monomers. This realization provides a convenient means of examining how other parameters such as particle size affect the activation energy and, thus, W. As depicted in Figure 7b by assuming a constant surface charge density (0.075 e/nm^2), E_a^* increases linearly with particle size when $E_a^* > 0$ ($C < 5$ mmol/L) and decreases linearly when $E_a^* < 0$. Hence, larger particles should display better stability in the reaction-limited regime, and smaller particles should have better stability in the diffusion-limited regime.

Moreover, from the change in E_a^* we can predict the effect of coatings on NPs. Generally, negatively charged moieties conjugated to the surface of a Au-NP, for example, should increase resistance to flocculation as it increases electrostatic repulsion and decreases van der Waals attraction.[4] The charge density of a conjugated Au-NP can be at least 10 times higher (>1 e/nm^2 when the surface packing density of singly charged molecules reached 5×10^{14} cm^{-2}) than that of an unconjugated Au-NP (0.075 e/nm^2),[1,33−35] contributing significantly to the electrostatic repulsion. By coating the colloids with a covalently bound negatively charged layer, colloidal stability may be improved because E_a^* is increased.

5. Conclusions

We have demonstrated a systematic approach to characterizing the aggregation of nanoparticles in solution with ES-DMA. This particle-sizing method has sufficient resolution to identify the aggregation state of NPs and to monitor changes in the number concentration as a function of ionic strength and reaction time. For the range of reaction times considered, we found the degree of aggregation to be proportional to the ionic strength and the residence time. From these data, we determined the surface potential and surface charge density of Au-NPs, values found to be consistent with those previously reported in the literature determined using other methods. A kinetic analysis of the ES-DMA data yields a rate constant and energy barrier for Au-NP aggregation. From these values, a critical salt concentration was obtained, and the boundary between the diffusion-limited and reaction-limited interactive potential regimes was found to be ~6.5 mmol/L.

(33) Kunze, J.; Burgess, I.; Nichols, R.; Buess-Herman, C.; Lipkowski, J. *J. Electroanal. Chem.* **2007**, *599*, 147–159.
(34) Kimura, K.; Takashima, S.; Ohshima, H. *J. Phys. Chem. B* **2002**, *106*, 7260–7266.
(35) Schreiber, F. *Prog. Surf. Sci.* **2000**, *65*, 151–256.